A Numerical Study of the Effect of Forced Convection on Mass Transport from a Thin Oblate Spheroid of Ice in Air

R. L. PITTER[1] AND H. R. PRUPPACHER

Dept. of Meteorology, University of California, Los Angeles 90024

A. E. HAMIELEC

Dept. of Chemical Engineering, McMaster University, Hamilton, Ontario, Canada

(Manuscript received 23 October 1973, in revised form 29 January 1974)

ABSTRACT

Numerical solutions have been found for the vapor density field around a simple ice plate, idealized as an oblate spheroid of axis ratio 0.05, having Reynolds numbers between 0.1 and 20, and falling in a fluid of Schmidt number 0.71. The present solutions are compared with experimental data after Thorpe and Mason for evaporating ice plates, the numerical results of Masliyah and Epstein for oblate spheroids of axis ratio 0.2, and the analytical results of Brenner for thin disks. It is shown that the ventilation coefficient varies linearly with $N_{Sc}^{\frac{1}{3}}N_{Re}^{\frac{1}{2}}$ at higher Reynolds numbers, while as the Reynolds number approaches zero it approaches its stationary value via the analytical solution of Brenner. Over the range of Reynolds numbers investigated, ventilation coefficients for thin oblate spheroids were found to be lower than those for spheres.

1. Introduction

In many clouds which form in continental air masses the drops are too small to grow by collision and coalescence with other drops. In such clouds, efficient growth of hydrometeors to precipitation size often commences when portions of the cloud become cold enough for ice crystals to nucleate and hence for glaciation to occur. The ice crystals formed usually grow in two stages: initially by diffusion of water vapor, and subsequently by riming. Ono (1969), Wilkins and Auer (1970), and Pitter and Pruppacher (1974) showed that, after nucleation, thin hexagonal ice plates must grow by vapor diffusion to at least 150 μm radius before riming may commence. Since the ice crystals are falling under the influence of gravity during their diffusional growth, a quantitative description of this growth mechanism must include the effects of forced convection.

Similarly, for a quantitative description of the evaporation of ice crystals falling in air which is subsaturated with respect to ice, one must consider the enhancement of mass transport from the falling crystals by forced convection. While the accurate determination of the diffusion growth rate of ice crystals allows prediction of the onset of riming, likewise an accurate knowledge of the rate of evaporation of ice crystals allows determination of their mass loss during their fall as single crystals or snowflakes from cloud to ground. The latter process is also of considerable importance in the prediction of the fall distance ice crystals may survive in ice-subsaturated air. Such will determine the ability of ice crystals falling from high cirrus clouds to nucleate supercooled cloud layers below (Braham, 1967).

Koenig (1968, 1971) and Jayaweera (1971) used the electrostatic analog theory to compute the diffusional growth of falling ice crystals. However, lacking any better results to apply, they used Sherwood numbers determined experimentally by Skelland and Cornish (1963) for thick oblate spheroids ($AR>0.3$). Numerous researchers have attempted to correlate experimental values of the mean Sherwood number $\overline{N_{Sh}}$ with corresponding values of the Reynolds number N_{Re} for forced convection around liquid drops or solid spheres evaporating in a gaseous environment, or solid spheres dissolving in a liquid (Ranz and Marshall, 1952; Garner and Suckling, 1958; Garner and Keey, 1958; Garner and Grafton, 1954; Frössling, 1938). These attempts suggested that the mean Sherwood number can be correlated to the quantity $N_{Sc}^{m}N_{Re}^{n}$, where $N_{Sc}=\nu/\mathfrak{D}$ is the Schmidt number. Results of experiments at high and intermediate Reynolds numbers have suggested that the correlation is linear at these Reynolds numbers, and takes the form

$$\overline{N_{Sh}}=C_1+C_2N_{Sc}^{m}N_{Re}^{n}, \tag{1}$$

where C_1, C_2, m and n are constants. C_1 in Eq. (1) does not represent the value of $\overline{N_{Sh}}$ at $N_{Re}=0$ since it cannot be assumed *a priori* that the relations found experi-

[1] Present affiliation: Department of Environmental Technology, Oregon Graduate Center for Study and Research, Beaverton 97005.

mentally at high and intermediate Reynolds numbers are valid at all Reynolds numbers down to zero. While numerous studies suggested that $m=\frac{1}{3}$ and $n=\frac{1}{2}$, the studies of Rowe *et al.* (1965) indicated that both exponents are functions of the Reynolds number, and that m is also a function of the Schmidt number, meaning that $\overline{N_{Sh}}$ does not vary linearly with $X=N_{Sc}^{\frac{1}{3}}N_{Re}^{\frac{1}{2}}$ over the entire range of Reynolds numbers. This was confirmed by Beard and Pruppacher (1971) who studied the evaporation of freely falling water drops in air by means of wind tunnel experiments. While $\overline{N_{Sh}}$ varied linearly with X at larger values of N_{Re}, at lower values it smoothly approached the value $\overline{N_{Sh_0}}=2$ by way of the analytical relation of $\overline{N_{Sh}}$ for creeping flow given by Acrivos and Taylor (1962). Since viscous flow past a body is critically dependent on the shape of that body, one might expect the dependence of the mean Sherwood number on N_{Sc} and N_{Re} to vary widely with shape. However, Pasternak and Gauvin (1960) showed for a wide variety of shapes (cylinders, prisms, cubes, hemispheres, etc.) that at high Reynolds numbers the mean Sherwood number could be related to the Reynolds number and Schmidt number by an equation of the form

$$\overline{N_{Sh}}=C_1+C_3N_{Sc}^{m}N_{Re(L^*)}^{n}, \tag{2}$$

with $m=\frac{1}{3}$ and $n\approx\frac{1}{2}$. The Reynolds number $N_{Re(L^*)}$ is based on the characteristic length L^*, defined as the ratio of the total surface area of the body to its perimeter normal to the direction of the flow. The results of Pasternak and Gauvin were verified by Skelland and Cornish (1963) for oblate spheroids of axis ratio >0.3 and Reynolds numbers between 100 and 6000. Since the surface area of an oblate spheroid is a function of the axis ratio, $N_{Re(L^*)}$ may be related to $N_{Re(2a)}$, which is the present definition of N_{Re}, by noting that

$$L^*=a\left[1+\frac{AR^2}{2e}\ln\left(\frac{1+e}{1-e}\right)\right], \tag{3}$$

and that the term in brackets varies from 1 for a very thin oblate spheroid to 2 for a sphere. Consequently,

$$N_{Re(L^*)}=\frac{1}{2}\left[1+\frac{AR^2}{2e}\ln\left(\frac{1+e}{1-e}\right)\right]N_{Re(2a)}. \tag{4}$$

Thus, for an oblate spheroid, a relation of the form

$$\overline{N_{Sh}}=C_1+C_3N_{Sc}^{m}N_{Re(L^*)}^{n} \tag{5}$$

is valid at intermediate and high Reynolds numbers.

In a recent study, Masliyah and Epstein (1971) numerically computed mean Sherwood numbers for oblate spheroids of axis ratio 0.2 at Reynolds numbers between 10 and 100 and N_{Sc} of 0.7. Their results showed that, for $m=\frac{1}{3}$, n was not constant but continuously decreased for increasing Reynolds numbers to reach a value of about 0.5 at Reynolds number 100. This means that, as in the case for a sphere, $\overline{N_{Sh}}$ for an oblate spheroid does not vary linearly with X over the entire range of Reynolds numbers, but it does approach a linear variation at higher Reynolds numbers. Brenner (1963) generalized the singular perturbation technique to examine mass transport for bodies of arbitrary shape in creeping flow ($N_{Re}\ll 1$). For a sphere, Brenner duplicated the results of Acrivos and Taylor,

$$\overline{N_{Sh}}=2+\tfrac{1}{2}N_{Pe}+\tfrac{1}{4}N_{Pe}^2\ln N_{Pe}, \tag{6}$$

where the Peclet number is $N_{Pe}=N_{Sc}N_{Re}$. For an infinitely thin circular disk, Brenner obtained

$$\overline{N_{Sh}}=\frac{4}{\pi}+\frac{2}{\pi^2}N_{Pe}+\frac{8}{3\pi^2}N_{Pe}^2\ln N_{Pe}. \tag{7}$$

Thorpe and Mason (1966) performed experimental studies of mass transfer from simple hexagonal plates of ice at $10\leqslant N_{Re}\leqslant 200$. Their results were expressed in terms of the ventilation coefficient (see Appendix A) as

$$f=0.65+0.44\left(\frac{1}{2}+\frac{h}{2a}\right)^{\frac{1}{2}}X, \tag{8}$$

where $h/2a$ is the aspect ratio of the ice crystal. If one assumes that the plates investigated were very thin ($h\ll a$), one finds that f varies linearly with X as

$$f=0.65+0.312X. \tag{9}$$

Again, it is emphasized that the first term on the right-hand side of Eq. (9) does not represent the value of f at Reynolds number zero, but is rather the f-intercept of the experimental results applicable to Reynolds numbers between 10 and 200. The results of Thorpe and Mason are somewhat suspect since the ice crystals were suspended on wires, which not only caused disturbances in the airflow, but also acted as an artificial means of heat transport to the crystal.

Jayaweera and Cottis (1969), and List and Schemenauer (1971) experimentally showed that the hydrodynamic behavior of a simple hexagonal plate can be approximated with sufficient accuracy by that of a circular disk, and Pitter *et al.* (1973) showed that the hydrodynamic behavior of a thin oblate spheroid is the same as that of a circular disk of the same aspect ratio. These results suggest that the mass transport from a ventilated thin hexagonal plate of Reynolds number between 0.01 and 100, typical for ice plates in atmospheric clouds, can be closely approximated by that from an oblate spheroid of the same aspect ratio.

Unfortunately, there are few reports in literature which directly apply to the above problem: The analytical results of Brenner for thin circular disks apply only to very low Reynolds numbers; the experimental results of Thorpe and Mason, as stated above, must be treated with caution; the numerical results of Masliyah and Epstein apply only to intermediate

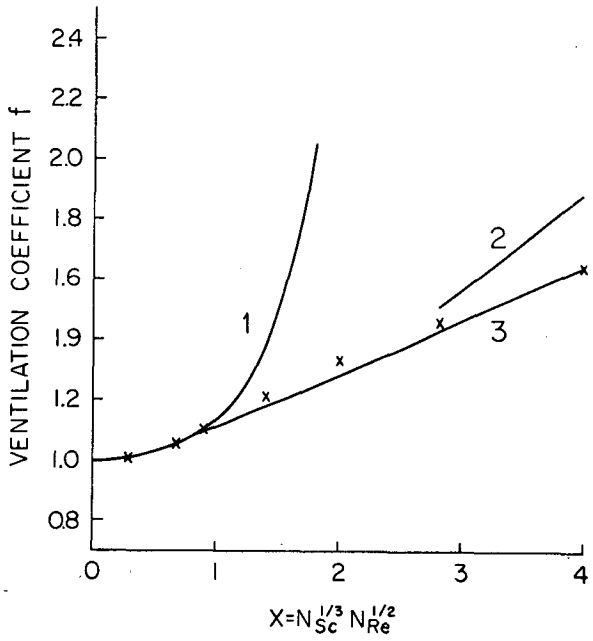

FIG. 1. Variation of ventilation coefficient f with X for thin disks and oblate spheroids: 1. Brenner, analytical, disk, $N_{Sc}=0.71$; 2. Thorpe and Mason, experimental, for thin disk; 3. present results (×'s) numerical, oblate spheroid, $AR=0.05$, $N_{Sc}=0.71$.

Reynolds numbers and to oblate spheroids of axis ratio $\geqslant 0.2$; and the experimental results of Skelland and Cornish can only be used at high Reynolds numbers.

These reasons prompted us to undertake a numerical study in order to obtain accurate values for the mean Sherwood numbers of thin oblate spheroids of low and intermediate Reynolds numbers. In this study, we used the flow fields previously determined by Pitter *et al.* (1973) to solve the vapor density continuity equation about an oblate spheroid of axis ratio 0.05 and Reynolds number between 0.1 and 20 moving in a fluid of $N_{Sc}=0.71$. From this solution, we determined the effect of forced convection on mass transport, as expressed by the mean Sherwood number and the ventilation coefficient.

2. Numerical model

The numerical value of the mean Sherwood number was obtained using Eq. (A12) after the vapor density field was relaxed using the vapor density continuity equation, given by Eq. (A19), with boundary conditions given by Eq. (A20). Solution was performed using either a CDC 6400 or IBM 360/91 computer. The meaning of the mean Sherwood number for an oblate spheroid, and the development and solution of the vapor density continuity equation are discussed in detail in Appendix A.

The numerical solution of the continuity equation [Eq. (A19)] in finite-difference form gave rise to truncation and grid size errors which caused small inaccuracies in the computed values of the ventilation coefficient and mean Sherwood number. Wall effects, arising from the finite domain size, must also be accounted for. At low Reynolds numbers, inertial effects are small, and consequently the effect of inertia on wall effects was neglected. Corrections were applied to ventilation coefficients and mean Sherwood numbers for cases of $N_{Re}\leqslant 1$. The correction method has been successfully used by LeClair *et al.* (1970) to correct for the effect of the same errors in numerically computed values of the drag force coefficient at low Reynolds numbers. This method estimates the correction to the computed value (either f or $\overline{N_{Sh}}$) by comparing the analytical solution of Brenner for creeping flow with infinitely distant walls and no finite-difference errors to the numerical solution for creeping flow with an outer boundary at a finite distance. Thus, for the ventilation coefficient

$$(f_{NS})_{num.}-(f_{NS})_{num.,corr.}=(f_{CF})_{num.}-(f_{CF})_{anal.}, \quad (10)$$

or

$$(f_{NS})_{num.,corr.}=(f_{NS})_{num.}-[(f_{CF})_{num.}-(f_{CF})_{anal.}], \quad (11)$$

and similarly for the mean Sherwood number. Subscripts NS and CF denote values based upon flow fields determined from the full Navier-Stokes equations of motion and from creeping flow. This correction lowered computed values about 4%. At $N_{Re}>1$, no corrections were applied.

3. Results

The numerical solution of the vapor density continuity equation was performed for oblate spheroids of axis ratio 0.05 and Reynolds numbers between 0.1 and 20. The Schmidt number was taken as 0.71, which is a reasonable value for atmospheric conditions. The results are presented in terms of the mean Sherwood number or the ventilation coefficient as a function of the parameter $X=N_{Sc}^{\frac{1}{3}}N_{Re}^{\frac{1}{2}}$. The present result are summarized in Table 1 and are plotted in Fig. 1 together with the experimental results of Thorpe and Mason and the analytical results of Brenner, both of which apply to a thin disk. It is seen from Fig. 1 that the present values for the ventilation coefficient of a thin oblate spheroid approach the analytical values of Brenner for creeping

TABLE 1. Mean Sherwood numbers and ventilation coefficients for oblate spheroids; $AR=0.05$, $N_{Sc}=0.71$ (present numerical results).

N_{Re}	X	N	r_∞	$\overline{N_{Sh}}$	f
0.1	0.282	39	19.2	1.324	1.009
0.5	0.632	35	15.7	1.375	1.048
1.	0.893	31	10.6	1.448	1.104
2.	1.41	31	10.6	1.599	1.218
5.	2.00	27	7.1	1.755	1.338
10.	2.82	27	7.1	1.928	1.465
20.	3.99	25	5.8	2.161	1.647

flow of a thin disk at low Reynolds numbers. This is analogous to the results of Beard and Pruppacher (1971) and Woo and Hamielec (1971), who showed that ventilation coefficient of a sphere approaches its value for a stationary sphere via the analytical values of Acrivos and Taylor. The experimental results of Thorpe and Mason are somewhat higher than the present numerical results. This is due possibly to the consequence of the suspension wires altering the heat balance from that which the crystal would experience while freely falling. Curve 3 of Fig. 1 depicts a reasonable fit through the present results. For $X \leqslant 0.71$ ($N_{Re} \leqslant 0.63$ at $N_{Sc}=0.71$) the ventilation coefficient is represented by Brenner's relation,

$$f=1+0.142X^2+0.054X^4 \ln(0.893X^2). \quad (12)$$

For $X \geqslant 0.71$, the ventilation coefficient is represented by the linear relation

$$f=0.937+0.178X. \quad (13)$$

In Fig. 2, a comparison is made between the present numerical results for oblate spheroids of axis ratio 0.05, the numerical results of Masliyah and Epstein for oblate spheroids of axis ratio 0.2, and those of Woo and Hamielec for spheres. The results vary in a consistent manner. At any particular Reynolds number, the sphere has the largest ventilation coefficient and the thin oblate spheroid (present results) the smallest, while the oblate spheroid of axis ratio 0.2 assumes an intermediate value. As the Reynolds number decreases to zero, the ventilation coefficients of all three bodies approach the limiting value at $N_{Re}=0$ in the same manner. This is reasonable since at low Reynolds numbers the flow field causes very little enhancement of mass transport, and consequently variations in flow fields around differently shaped bodies yield negligible variations in the ventilation coefficients. As the Reynolds number increases, the variation in the ventilation coefficients between various shapes steadily increases. There is a transparent physical basis for the ventilation coefficient to be larger for a sphere than for a thin oblate spheroid at any of the Reynolds numbers considered here. At Reynolds number between 1 and 2 (X between 0.9 and 1.4), the thin oblate spheroid has developed an eddy at its downstream end. As a consequence of its very thin shape, the eddy rapidly expands to encompass the entire back half of the body. Around the sphere, fluid is advected and remains close to the body over all the surface area. The thin oblate spheroid experiences such only over the fore half of its surface. The eddy in the rear of the thin oblate spheroid, although still allowing some enhancement over the unventilated case, is unable to transport mass to (or from) the surrounding fluid at the same rate as the front half. Consequently, the ventilation coefficient for a thin oblate spheroid is lower, since the forced convection mechanism is not able to operate efficiently over the entire surface area of the body.

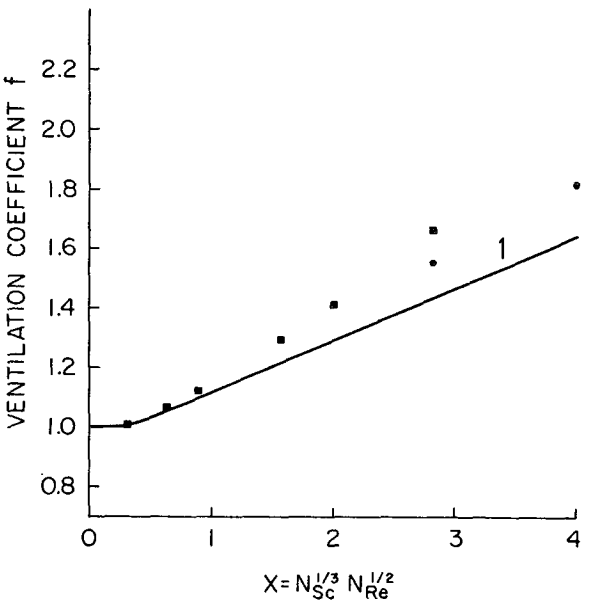

FIG. 2. Variation of ventilation coefficient with X for spheres (Woo and Hamielec, squares) and oblate spheroids [$AR=0.2$ (Masliyah and Epstein, circles) and $AR=0.05$, curve 1 (present results)].

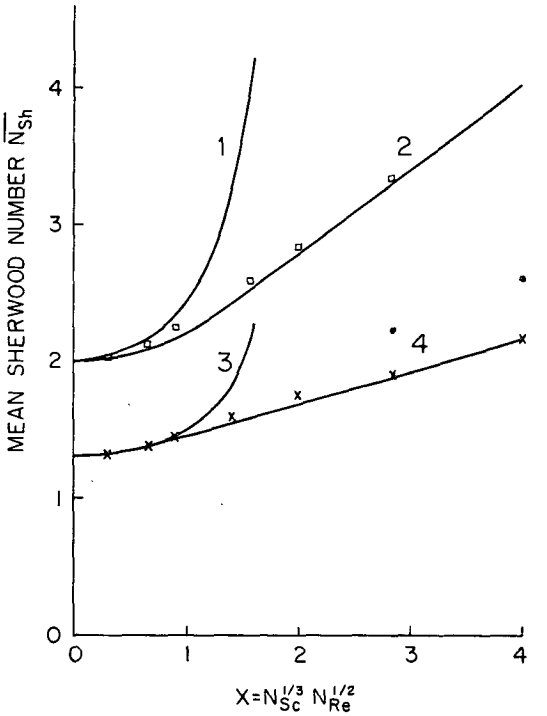

FIG. 3. Variation of mean Sherwood number with X ($N_{Sc}=0.71\pm0.01$): 1. Brenner, sphere, analytical; 2. Beard and Pruppacher, sphere, experimental; 3. Brenner, thin disk, analytical; 4. present results (X's), oblate spheroid, $AR=0.05$, numerical; squares (Woo and Hamielec) sphere, numerical; dots (Masliyah and Epstein) oblate spheroid, $AR=0.2$, numerical.

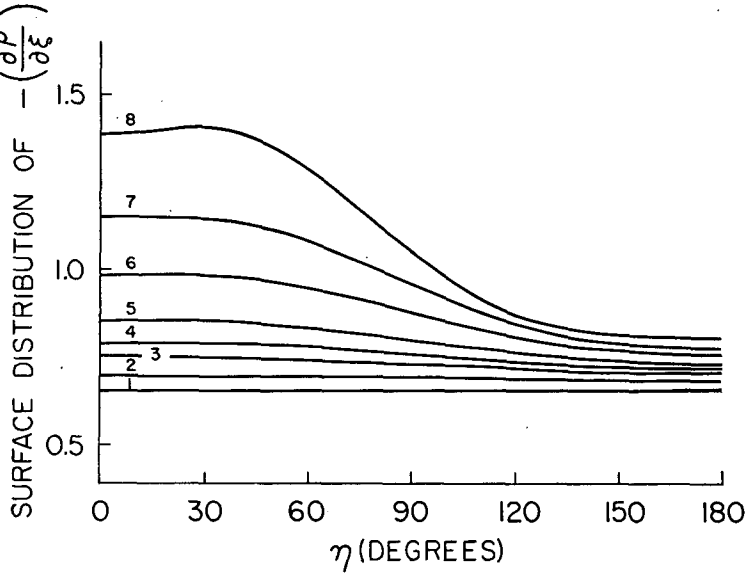

FIG. 4. Variation of $-(\partial\rho^*/\partial\xi)_{\xi_0,\eta}$ with η for oblate spheroid of axis ratio 0.05 (present results) 1. $N_{Re}=0$; 2. $N_{Re}=0.1$; 3. $N_{Re}=0.5$; 4. $N_{Re}=1$; 5. $N_{Re}=2$; 6. $N_{Re}=5$; 7. $N_{Re}=10$; 8. $N_{Re}=20$.

In Fig. 3, the results are plotted in terms of the mean Sherwood number versus X. It is apparent that, irrespective of shape, the mean Sherwood number approaches its unventilated value via its respective analytical results, while at higher Reynolds numbers the relation between $\overline{N_{Sh}}$ and X becomes linear.

Fig. 4 shows the process of enhanced ventilation in more detail by investigating the surface distribution of the vapor density derivative normal to the surface of the thin oblate spheroid (present results). At Reynolds number zero, analytical results produce a normal vapor density derivative which is constant over the entire surface [see Eq. (A24)]. At low Reynolds numbers, there is a slight increase of the magnitude of the normal vapor density derivative over the case of Reynolds number zero, and a very slight variation of the magnitude of the derivative with polar angle. At intermediate Reynolds numbers, as the Reynolds number increases, the magnitude of the derivative increases in the front half of the oblate spheroid, but there is only a minimal increase in the rear half due to the action of the eddy serving as a very thick boundary layer and thus restricting mass transport in that region. The results shown in Fig. 4 support the earlier statement that the eddy at the rear of the thin oblate spheroid at Reynolds numbers between 1 and 20 serves to diminish the area of effective mass transport to the advected environmental fluid. Since the sphere forms an eddy at Reynolds number 20, there is much less variation in the magnitude of the normal vapor density derivative with angle at lower Reynolds numbers, and consequently the sphere possesses a greater enhancement of mass transport than does a thin oblate spheroid at the same Reynolds number. The same argument justifies the intermediate enhancement of thick oblate spheroids.

For a lack of better values on the ventilation coefficient for falling plate-like ice crystals, previous computations on the rate of evaporation (Braham and Spyers-Duran, 1967) and on the rate of diffusional growth (Koenig, 1968, 1971; Jayaweera, 1971) of plate-like ice crystals either were based on values for a sphere or relied on the rather crude measurements of Thorpe and Mason (1966) or the experiments of Skelland and Cornish (1963) which only apply to rather thick oblate spheroids of axis ratio >0.3. Our Eqs. (12) and (13) for the variation of the ventilation coefficient f of thin plate-like ice crystals falling in air provide more accurate values for f than those available from previous studies. Thus, it is hoped that previous and future computations on the diffusional growth and evaporation of ice crystals will be checked in the light of the new information presented in this article.

Acknowledgments. Two of the authors (R. L. P. and H. R. P.) are indebted to the National Science Foundation through Grant NSF GA 32814X, and the third author (A. E. H.) is indebted to the National Research Council of Canada for supporting the research presented in this paper.

APPENDIX A

Theory and Computation of the Sherwood Number

In order to examine the theory of the mean Sherwood number and ventilation coefficient for an oblate spheroid, we shall proceed in a similar manner as Woo

and Hamielec (1971)[2] did for a sphere. Considering a system of water vapor and dry air, Fick's first law of diffusion in a binary system from a fixed frame of reference can be expressed in terms of the mass flux of the water vapor (Bird *et al.*, 1960) as[3]

$$\rho_v \mathbf{V}_v = -\rho \mathfrak{D} \nabla (\rho_v/\rho) + (\rho_v/\rho)(\rho_v \mathbf{V}_v + \rho_d \mathbf{V}_d). \quad \text{(A1)}$$

At the surface of the oblate spheroid ($\xi = \xi_0$), $\rho_d \mathbf{V}_d = 0$ due to the dual boundary conditions of no slip at the surface and no flow through the interface, and thus the radial component of the water vapor flux at the surface of the oblate spheroid is

$$(\rho_v V_{v\xi})_{\xi_0} = \frac{-\rho \mathfrak{D}\left[h \frac{\partial}{\partial \xi}\left(\frac{\rho_v}{\rho}\right)\right]_{\xi_0}}{(1-\rho_v/\rho)_{\xi_0}}, \quad \text{(A2)}$$

where ρ and $\mathfrak{D}$ are assumed constant everywhere in space. The metric coefficient h arises from the expression of the gradient in curvilinear space. Integrating Eq. (A2) over the surface, one obtains the growth rate

$$\int_s (\rho_v V_{v\xi})_{\xi_0} dS = -\frac{dm}{dt} = \frac{-\rho \mathfrak{D} \int_s \left[h \frac{\partial}{\partial \xi}\left(\frac{\rho_v}{\rho}\right)\right]_{\xi_0} dS}{(1-\rho_v/\rho)_{\xi_0}}. \quad \text{(A3)}$$

Brenner (1963) defined the mean Sherwood number for an arbitrary body of revolution with radius a as

$$\overline{N_{\mathrm{Sh}}} = kA_{\mathrm{sfc}}/(2\pi a \mathfrak{D}), \quad \text{(A4)}$$

where k is the mean mass transport coefficient, which Bird *et al.* express for a binary system as

$$k = \frac{-(dm/dt)(1-\rho_v/\rho)_{\xi_0}}{\rho A_{\mathrm{sfc}} \Delta(\rho_v/\rho)}, \quad \text{(A5)}$$

where

$$\Delta(\rho_v/\rho) = (\rho_{v\xi_0}/\rho_{\xi_0}) - (\rho_{v\infty}/\rho_\infty). \quad \text{(A6)}$$

Combining Eqs. (A3)–(A5), the mean Sherwood number for an oblate spheroid is rewritten as

$$\overline{N_{\mathrm{Sh}}} = \frac{-(dm/dt)(1-\rho_v/\rho)_{\xi_0}}{2\pi a \rho \mathfrak{D} \Delta(\rho_v/\rho)}, \quad \text{(A7)}$$

or

$$\overline{N_{\mathrm{Sh}}} = \frac{-\int_s \left[h \frac{\partial}{\partial \xi}\left(\frac{\rho_v}{\rho}\right)\right]_{\xi_0} dS}{2\pi a \Delta(\rho_v/\rho)}. \quad \text{(A8)}$$

A dimensionless, normalized vapor density ρ^* is introduced here, defined as

$$\rho^* = (\rho_v - \rho_{v\infty})/(\rho_{v\xi_0} - \rho_{v\infty}). \quad \text{(A9)}$$

Eq. (A8) then becomes

$$\overline{N_{\mathrm{Sh}}} = \frac{-\int_s \left[h \frac{\partial \rho^*}{\partial \xi}\right]_{\xi_0} dS}{2\pi a}. \quad \text{(A10)}$$

Since the surface integral may be expressed as

$$\int_s dS = 2\pi a \int_0^\pi \left[\frac{1}{h}\right]_{\xi_0} \sin\eta d\eta, \quad \text{(A11)}$$

Eq. (A10) is rewritten

$$\overline{N_{\mathrm{Sh}}} = -\int_0^\pi \left[\frac{\partial \rho^*}{\partial \xi}\right]_{\xi_0} \sin\eta d\eta. \quad \text{(A12)}$$

Thus, in order to compute the mean Sherwood number for an oblate spheroid, it is necessary first to determine the surface distribution of the normal derivative of the vapor density. The steady-state continuity equation for water vapor is

$$\nabla \cdot (\rho_v \mathbf{V}_v) = 0, \quad \text{(A13)}$$

and consequently, since $\mathbf{V} = (\rho_v \mathbf{V}_v + \rho_d \mathbf{V}_d)/\rho$, substitution of (A1) into (A13) yields

$$\nabla \cdot (\rho_v \mathbf{V}_v) = 0 = \rho_v \nabla \cdot \mathbf{V} + \mathbf{V} \cdot \nabla \rho_v = \nabla \cdot [\rho \mathfrak{D} \nabla (\rho_v/\rho)]. \quad \text{(A14)}$$

Since ρ is assumed constant, the continuity equation for moist air reduces to $\nabla \cdot \mathbf{V} = 0$, and Eq. (A14) reduces to

$$\mathbf{V} \cdot \nabla \rho_v = \mathfrak{D} \nabla^2 \rho_v. \quad \text{(A15)}$$

Nondimensionalization is accomplished by defining the parameters

$$\left.\begin{aligned} \mathbf{V}^* &= \mathbf{V}/V_\infty \\ \nabla^* &= a\nabla \\ N_{\mathrm{Pe}} &= N_{\mathrm{Re}} N_{\mathrm{Sc}} = 2aV_\infty/\mathfrak{D}. \end{aligned}\right\} \quad \text{(A16)}$$

Eq. (A15) then becomes

$$\tfrac{1}{2} N_{\mathrm{Pe}} \mathbf{V}^* \cdot \nabla^* \rho^* = \overset{*}{\nabla}{}^2 \rho^*. \quad \text{(A17)}$$

For steady flow, the nondimensional streamfunction ψ^* is defined by the relation

$$\mathbf{V}^* = \frac{\mathbf{e}_\varphi}{y^*} \times \overset{*}{\nabla} \psi^*, \quad \text{(A18)}$$

where $y^* = \operatorname{sech}\xi_0 \cosh\xi \sin\eta$ is the normal distance from the axis of symmetry. Consequently, (A17) reduces to

$$\frac{N_{\mathrm{Pe}}}{2y^*} J_{\xi,\eta}(\psi^*, \rho^*) = \overset{*}{\nabla}{}^2 \rho^*. \quad \text{(A19)}$$

The normalized vapor density is subject to the following

[2] Note that in their work as the result of a printing error the right-hand sides of Eqs. (30) and (31) are off by factors of $\frac{1}{2}$ and 2, respectively.

[3] See List of Symbols (Appendix B).

boundary conditions:

$$\left.\begin{aligned} \xi=\xi_0: &\quad \rho^*=1 \\ \xi=\xi_\infty: &\quad \rho^*=0 \\ \eta=0,\pi: &\quad \frac{\partial\rho^*}{\partial\eta}=0 \end{aligned}\right\}. \tag{A20}$$

For a stationary oblate spheroid, (A19) becomes

$$\nabla^2\rho^*=0, \tag{A21}$$

which, as described by Morse and Feshbach (1953), has the solution

$$\rho^*=\frac{Q_0(i\xi)}{Q_0(i\xi_0)}, \tag{A22}$$

where Q_0 is the second Legendre polynomial

$$Q_0(i\xi)=\ln\left[\frac{i\xi+1}{i\xi-1}\right]. \tag{A23}$$

It is noted from Eq. (A22) that at $N_{Re}=0$, ρ^* has no η-dependence. For an oblate spheroid of axis ratio 0.05, solution of (A22) yields

$$\left.\frac{d\rho^*}{d\xi}\right|_{\xi_0}=-0.656, \tag{A24}$$

and subsequent substitution of this into (A12) yields

$$\overline{N_{Sh_0}}=1.312. \tag{A25}$$

From (A3) for $N_{Re}=0$, with ρ constant,

$$-\left(\frac{dm}{dt}\right)_0=\frac{-4\pi a\mathfrak{D}}{(1-\rho_v/\rho)_{\xi_0}}\left[\frac{\partial\rho^*}{\partial\xi}\right]_{\xi_0,0}, \tag{A26}$$

and consequently, from (A7),

$$\overline{N_{Sh}}=-2\left[\frac{\partial\rho^*}{\partial\xi}\right]_{\xi_0,0}\frac{dm/dt}{(dm/dt)_0}. \tag{A27}$$

It is interesting to compare the above results with those obtained from an approach frequently used in cloud physics literature (Mason, 1971). In this approach the electrostatic analog is used to determine the mass flux from a non-spherical ice crystal. Neglecting the last term on the right-hand side of Eq. (A1) since $\rho_v\ll\rho$, one finds for a stationary crystal

$$\left(\frac{dm}{dt}\right)_0=-4\pi C\mathfrak{D}(\rho_{v\xi_0}-\rho_{v\infty}), \tag{A28}$$

where C is the electrostatic capacitance, in units of length, for the particular ice crystal shape considered. Koenig (1968, 1971) and Jayaweera (1971) followed the suggestions of Pasternak and Gauvin (1960) to define the mean Sherwood number in terms of a shape parameter $L^*=A_{sfc}/P$. Thus, for the mean Sherwood number, they wrote

$$\overline{N_{Sh}}=\frac{-L^*(dm/dt)}{A_{sfc}\mathfrak{D}(\rho_{v\xi_0}-\rho_{v\infty})}, \tag{A29}$$

or

$$\overline{N_{Sh}}=\frac{-(dm/dt)}{P\mathfrak{D}(\rho_{v\xi_0}-\rho_{v\infty})}, \tag{A30}$$

where P is the perimeter of the body considered. For a body of revolution, $P=2\pi a$. Eq. (A30) becomes

$$\overline{N_{Sh}}=\frac{-(dm/dt)}{2\pi a\mathfrak{D}(\rho_{v\xi_0}-\rho_{\infty v})}, \tag{A31}$$

and Eq. (A29) may be expressed as

$$\frac{dm}{dt}=-\overline{N_{Sh}}2\pi a\mathfrak{D}(\rho_{v\xi_0}-\rho_{v\infty}). \tag{A32}$$

If the body is stationary, $dm/dt=(dm/dt)_0$ and $\overline{N_{Sh}}=\overline{N_{Sh_0}}$. Comparison of (A29) with (A28) then yields

$$\overline{N_{Sh_0}}=\frac{4\pi CL^*}{A_{sfc}}=4\pi C/P. \tag{A33}$$

For a sphere, $P=2\pi a$ and $C=a$, so $\overline{N_{Sh_0}}=2$. Similarly for a thin disk, $P=2\pi a$ and $C=2a/\pi$, so $\overline{N_{Sh_0}}=4/\pi=1.27$. From Eqs. (A28) and (A31),

$$\overline{N_{Sh}}=\frac{2C}{a}\frac{dm/dt}{(dm/dt)_0}. \tag{A34}$$

The electrostatic capacitance of an oblate spheroid is (Mason, 1971)

$$C=\frac{ae}{\cos^{-1}e}. \tag{A35}$$

For an oblate spheroid of $AR=0.05$, $C=0.656a$, and Eq. (A34) becomes

$$\frac{dm}{dt}=\frac{\overline{N_{Sh}}}{1.312}\left(\frac{dm}{dt}\right)_0, \tag{A36}$$

in agreement with Eq. (A25). Similarly, such treatment for a sphere yields

$$\frac{dm}{dt}=\frac{\overline{N_{Sh}}}{2}\left(\frac{dm}{dt}\right)_0. \tag{A37}$$

Similar to Frössling (1938), Thorpe and Mason (1966) defined a ventilation factor, or ventilation coefficient, for a hexagonal plate in order to measure the enhancement due to ventilation of the mass transport

over the stationary case; the coefficient f is given as

$$f=\frac{dm/dt}{(dm/dt)_0}. \tag{A38}$$

It is noted that the ventilation coefficient for an oblate spheroid may be written

$$f=\overline{N_{Sh}}/(2C^*), \tag{A39}$$

where $C^*=C/a$.

In the present investigation, the mean Sherwood number was determined from (A12) after solving (A19) with the boundary conditions of (A20). $\nabla^2\rho$ (with the asterisk deleted hereafter for convenience) was obtained from the relation

$$\nabla^2\rho=\frac{\partial^2\rho}{\partial\xi^2}+\tanh\xi\frac{\partial\rho}{\partial\xi}+\frac{\partial^2\rho}{\partial\eta^2}+\cot\eta\frac{\partial\rho}{\partial\eta}. \tag{A40}$$

The iterative continuity equation was expressed as

$$\begin{aligned}\rho^{n+1}(I,J)=\left[\frac{0.5A^2B^2}{A^2+B^2}\right]\Bigg[&\rho^n(I,J+1)\left\{\frac{1}{A^2}+\frac{\tanh\xi(J)}{2A}+\frac{N_{Pe}}{8AB}[\psi(I+1,J)-\psi(I-1,J)]\right\}\\&+\rho^n(I,J-1)\left\{\frac{1}{A^2}-\frac{\tanh\xi(J)}{2A}-\frac{N_{Pe}}{8AB}[\psi(I+1,J)-\psi(I-1,J)]\right\}\\&+\rho^n(I+1,J)\left\{\frac{1}{B^2}+\frac{\cot\eta(I)}{2B}-\frac{N_{Pe}}{8AB}[\psi(I,J+1)-\psi(I,J-1)]\right\}\\&+\rho^n(I-1,J)\left\{\frac{1}{B^2}-\frac{\cot\eta(I)}{2B}+\frac{N_{Pe}}{8AB}[\psi(I,J+1)-\psi(I,J-1)]\right\}\Bigg].\end{aligned} \tag{A41}$$

The grid used for relaxing the vapor density field consisted of 31 angular steps of size $B=6°$, and had radial step size of $A=0.1$. The number of radial steps, N, was chosen to yield an outer boundary sufficiently remote that the normal derivative of the vapor density at the surface of the oblate spheroid was not affected by the position of the outer boundary. Values of N and r_∞ are given in Table 1. An arbitrary ρ field was initially generated, from which the solution field was relaxed. From Eq. (A41) the residual was determined by

$$\Re^n(I,J)=\frac{\rho^{n+1}(I,J)-\rho^n(I,J)}{\rho^{n+1}(I,J)}, \tag{A42}$$

from which the vapor density was updated,

$$\rho^{n+1}(I,J)=\rho^n(I,J)+\gamma(I,J)\Re^n(I,J). \tag{A43}$$

Values of $\gamma(I,J)$ were critical to the efficiency of convergence, and were chosen in the manner of Woo (1971). The boundary conditions from Eq. (A20) were treated as follows. Along the oblate spheroid surface,

$$\rho(I,1)=1, \tag{A44}$$

at the outer boundary,

$$\rho(I,N)=0, \tag{A45}$$

and at the axis of symmetry, boundary values were updated using a finite-difference scheme of fourth-order accuracy,

$$\left.\begin{aligned}\rho^{n+1}(1,J)&=[18\rho^n(2,J)-9\rho^n(3,J)+2\rho^n(4,J)]/11\\ \rho^{n+1}(MP1,J)&=[18\rho^n(M,J)-9\rho^n(M-1,J)\\&\quad+2\rho^n(M-2,J)]/11\end{aligned}\right\}. \tag{A46}$$

The vapor density field was considered converged when the largest magnitude of the residual during an iteration was less than 0.01.

APPENDIX B

List of Symbols

A	radial step size
a	semi-major axis length
A_{sfc}	surface area
AR	axis ratio $[=b/a]$
B	angular step size
b	semi-major axis length
C	electrostatic capacitance
d	subscript denoting dry air
$\mathfrak{D}$	diffusivity of water vapor in air
e	eccentricity $[=(1-AR^2)^{\frac{1}{2}}]$
$\mathbf{e}_\varphi$	azimuthal unit vector
f	ventilation coefficient
h	metric coefficient $\{=[a\,\mathrm{sech}\xi_0(\sinh^2\xi+\cos^2\eta)^{\frac{1}{2}}]^{-1}\}$
I	polar angle index
J	radial coordinate index
$J_{\xi,\eta}$	Jacobian $J_{\xi,\eta}(\psi,\rho)=(\partial\psi/\partial\xi)(\partial\rho/\partial\eta)-(\partial\psi/\partial\eta)(\partial\rho/\partial\xi)$
k	mean mass transport coefficient
L^*	characteristic length $[=A_{sfc}/P]$
M	number of angular steps in grid, less one
$MP1$	number of angular steps in grid $[=M+1]$
N	number of radial steps in grid
n	iteration index
N_{Pe}	Peclet number $[=N_{Re}N_{Sc}=2aV_\infty/\mathfrak{D}]$
N_{Re}	Reynolds number $[=N_{Re(2a)}=2aV_\infty/\nu]$

$N_{\mathrm{Re}(L^*)}$ Reynolds number based on characteristic length $[=L^*V_\infty/\nu]$
N_{Sc} Schmidt number $[=\nu/\mathfrak{D}]$
$\overline{N_{\mathrm{Sh}}}$ mean Sherwood number
P perimeter of body normal to direction of flow
Q_0 second Legendre polynomial
$\mathfrak{R}$ residual
r_∞ normalized outer boundary distance from equator of oblate spheroid
$\mathbf{V}$ velocity
v subscript denoting water vapor
X parameter $[=N_{\mathrm{Sc}}N_{\mathrm{Re}}]$
y distance from axis of symmetry
γ relaxation coefficient
η angular coordinate
ξ radial coordinate
ξ_0 subscript denoting value at surface of oblate spheroid
ρ, ρ_v, ρ_d vapor density of air, water vapor, and dry air, respectively
φ azimuthal coordinate
ψ streamfunction
∇ nabla operator
∞ subscript denoting environmental value or value at outer boundary

REFERENCES

Acrivos, A., and T. D. Taylor, 1962: Heat and mass transfer from single spheres in Stokes flow. *Phys. Fluids*, **5**, 387–394.

Beard, K. V., and H. R. Pruppacher, 1971: A wind tunnel investigation of the rate of evaporation of small drops falling at terminal velocity in air. *J. Atmos. Sci.*, **28**, 1455–1464.

Bird, R. B., W. E. Stewart and E. N. Lightfoot, 1960: *Transport Phenomena*. New York, Wiley, 780 pp.

Braham, R. R., Jr., 1967: Cirrus cloud seeding as a trigger for storm development. *J. Atmos. Sci.*, **24**, 311–312.

——, and P. Spyers-Duran, 1967: Survival of cirrus crystals in clear air. *J. Appl. Meteor.*, **6**, 1053–1061.

Brenner, H., 1963: Forced convection heat and mass transfer at small Peclet numbers from a particle of arbitrary shape. *Chem. Eng. Sci.*, **18**, 109–122.

Frössling, N., 1938: Ueber die Verdunstung fallender Tropfen. *Beitr. Geophys.*, **52**, 170–216.

Garner, F. H., and R. W. Grafton, 1954: Mass transfer in fluid flow from a solid sphere. *Proc. Roy. Soc. London*, **A224**, 64–82.

——, and R. B. Keey, 1958: Mass transfer from single solid spheres. *Chem. Eng. Sci.*, **9**, 119–129.

——, and R. D. Suckling, 1958: Mass transfer from soluble solid spheres. *AIChE J.*, **4**, 114–124.

Jayaweera, K. O. L. F., 1971: Calculations of ice crystal growth. *J. Atmos. Sci.*, **28**, 728–736.

——, and R. E. Cottis, 1969: The fall velocities of plate-like and columnar ice crystals. *Quart. J. Roy. Meteor. Soc.*, **95**, 703–709.

Koenig, L. R., 1968: Numerical modeling of ice deposition. Memo. RM-5715-NSF, The Rand Corp., Santa Monica, Calif., 36 pp.

——, 1971: Numerical modeling of ice deposition. *J. Atmos. Sci.*, **28**, 226–237.

LeClair, B. P., A. E. Hamielec and H. R. Pruppacher, 1970: A numerical study of the drag on a sphere at low and intermediate Reynolds numbers. *J. Atmos. Sci.*, **27**, 308–315.

List, R., and R. S. Schemenauer, 1971: Free-fall behavior of planar snow crystals, conical grapel and small hail. *J. Atmos. Sci.*, **28**, 110–115.

Masliyah, J. H., and N. Epstein, 1971: Numerical solution of heat and mass transfer from spheroids in steady axisymmetric flow. *Proc. Intern. Symposium on Two-Phase Systems*, Haifa, Israel.

Mason, B. J., 1971: *The Physics of Clouds*, 2nd ed. Oxford, Clarendon Press, 671 pp.

Morse, P. M., and H. Feshbach, 1953: *Methods of Theoretical Physics*. New York, McGraw-Hill, 1939 pp.

Ono, A., 1969: The shape and riming properties of ice crystals in natural clouds. *J. Atmos. Sci.*, **26**, 138–147.

Pasternak, I. S., and W. H. Gauvin, 1960: Turbulent heat and mass transfer from stationary particles. *Can. J. Chem. Eng.*, **38**, 35–42.

Pitter, R. L., and H. R. Pruppacher, 1974: A numerical investigation of collision efficiencies of simple ice plates colliding with supercooled water drops. *J. Atmos. Sci.*, **31** (in press).

——, —— and A. E. Hamielec, 1973: A numerical study of viscous flow past a thin oblate spheroid at low and intermediate Reynolds numbers. *J. Atmos. Sci.*, **30**, 125–134.

Ranz, W. E., and W. R. Marshall, 1952: Evaporation from drops, Part 2. *Chem. Eng. Prog.*, **48**, 173–180.

Rowe, P. N., K. T. Claxton and J. B. Lewis, 1965: Heat and mass transfer from a single sphere in an extensive flowing fluid. *Trans. Inst. Chem. Engrs. London*, **43**, T14–T31.

Skelland, A. H. P., and A. R. H. Cornish, 1963: Mass transfer from spheroids to an air stream. *AIChE J.*, **9**, 73–76.

Thorpe, A. D., and B. J. Mason, 1966: The evaporation of ice spheres and ice crystals, *Brit. J. Appl. Phys.*, **17**, 541–548.

Wilkins, R. D., and A. H. Auer, 1970: Riming properties in hexagonal ice crystals. *Preprints Conf. Cloud Physics*, Fort Collins, Colo., Amer. Meteor. Soc., 81–82.

Woo, S., 1971: Simultaneous free and forced convection around submerged cylinders and spheres. Ph.D. dissertation, McMaster University, Hamilton, Canada, 224 pp.

——, and A. E. Hamielec, 1971: A numerical method of determining the rate of evaporation of small water drops falling at terminal velocity in air. *J. Atmos. Sci.*, **28**, 1448–1454.